2018 European Control Conference (ECC)
June 12-15, 2018. Limassol, Cyprus

On-Off Quantization of an MPC Policy for Coupled Station Keeping, Attitude Control, and Momentum Management of GEO Satellites

Ryan J. Caverly[1], Stefano Di Cairano[2], and Avishai Weiss[2]

Abstract— **This paper introduces a novel on-off quantization scheme used with a control architecture based on model predictive control (MPC) to simultaneously perform station keeping, attitude control, and momentum management of a nadir-pointing geostationary satellite equipped with three reaction wheels and four on-off electric thrusters. The MPC policy includes an inner-loop $SO(3)$-based attitude control law to maintain a nadir-pointing attitude, and an outer loop for station keeping and momentum management. The continuous thrust command generated by the MPC policy is quantized as a single on-off pulse every feedback period in such a way that the predicted error in the states induced by quantization is minimized. This quantization scheme introduces very limited change in behavior and performance compared to results with the non-quantized MPC policy, and uses significantly less on-off pulses compared to other approaches in the literature, such as pulse-width modulation. The tuning parameters of the proposed quantization scheme are discussed in detail and their effects on closed-loop performance are analyzed numerically.**

I. Introduction

Advancement of low-thrust electric propulsion technology has led to its deployment in a range of satellite applications, including station keeping of geostationary Earth orbit (GEO) satellites [1]. Station keeping maneuvers with chemical propulsion are typically commanded manually from a ground station roughly once every two weeks, in order to counteract orbital perturbations and keep the satellite within a station keeping window. The thrust magnitude of electric propulsion is significantly less than chemical propulsion, which prevents the use of traditional station keeping techniques, as maneuvers must be performed more frequently with limited thrust magnitude. Autonomous control strategies have been developed for satellite orbital maintenance with electric propulsion [2–10]. Model predictive control (MPC) policies for simultaneous station keeping, attitude control, and momentum management are presented in [7–9].

Many electric propulsion systems are not capable of throttling thrust and only operate with on-off pulses, which must be considered in spacecraft control policies. One approach is to incorporate quantized control directly within the control policy, as done in [3]. However, this leads to a mixed-integer linear program, which is computationally expensive and difficult to implement in real time, especially onboard a satellite computing platform. A more popular approach is to have a control policy compute continuous thrust commands and a quantization scheme transform these commands into on-off thrust pulses [4–7]. A well-designed quantization scheme has very little impact on the performance of the system compared to the nominal non-quantized performance. Although the pulse-width modulation (PWM) quantized control policies in [4–7] are capable of yielding very similar Δv to non-quantized versions of their respective control policies, they require a large number of on-off thruster pulses. For example, the MPC policy with PWM quantization in [7] uses an average of 30 pulses per thruster per orbit, which is an order of magnitude more than the number of on-off cycles that current electric thrusters are capable of for a typical 15 year lifespan of a satellite in GEO [11].

This paper presents a novel quantization scheme for a control policy that simultaneously performs station keeping, attitude control, and momentum management of a GEO satellite. A single-pulse quantization scheme is implemented every feedback period, which may be larger than a single controller time step. A single on-off thrust pulse is made possible by minimizing the predicted error in the states induced by quantization when solving for the on and off thrust times, which also serves to minimize deviation in closed-loop system behavior caused by quantization. A preliminary version of the work presented in this paper is found in [9], which is expanded with details regarding the quantization scheme and analysis of the effect on performance of the quantization scheme parameters, including the thrust cutoff value, the number of discretization time steps between feedback, and the weighting matrix used in the minimization of the predicted state error. The paper begins in Section II with the problem statement and satellite model. Section III describes the MPC policy and the proposed single-pulse thruster quantization scheme. Simulation results studying the effect of varying quantization scheme parameters are presented in Section V and closing remarks are fin Section VI.

A. Preliminaries and Notation

The following notation is used throughout the paper. A reference frame $\mathcal{F}_a$ is defined by a set of three orthonormal dextral basis vectors, $\{\underrightarrow{a}^1, \underrightarrow{a}^2, \underrightarrow{a}^3\}$. An arbitrary physical vector, denoted as $\underrightarrow{v}$, is resolved in $\mathcal{F}_a$ as $\mathbf{v}_a$, where $\mathbf{v}_a^\mathsf{T} = \begin{bmatrix} v_{a1} & v_{a2} & v_{a3} \end{bmatrix}$ and $\underrightarrow{v} = v_{a1}\underrightarrow{a}^1 + v_{a2}\underrightarrow{a}^2 + v_{a3}\underrightarrow{a}^3$. The mapping between a physical vector resolved in different reference frames is given by the direction cosine matrix (DCM) $\mathbf{C}_{ba} \in SO(3)$, where $SO(3) = \{\mathbf{C} \in \mathbb{R}^{3\times 3} \,|\, \mathbf{C}^\mathsf{T}\mathbf{C} = \mathbf{1}, \det(\mathbf{C}) = +1\}$ and $\mathbf{1}$ is the identity matrix. For example, $\mathbf{v}_b = \mathbf{C}_{ba}\mathbf{v}_a$, where $\mathbf{v}_b$ is $\underrightarrow{v}$ resolved in $\mathcal{F}_b$ and $\mathbf{C}_{ba}$ represents

[1] R. J. Caverly is with the Department of Aerospace Engineering, University of Michigan, Ann Arbor, MI 48109, USA. Email: caverly@umich.edu. He was an intern at MERL during the development of this work.

[2] S. Di Cairano and A. Weiss are with Mitsubishi Research Laboratories, Cambridge, MA 02139, USA. Emails: {dicairano,weiss}@merl.com.

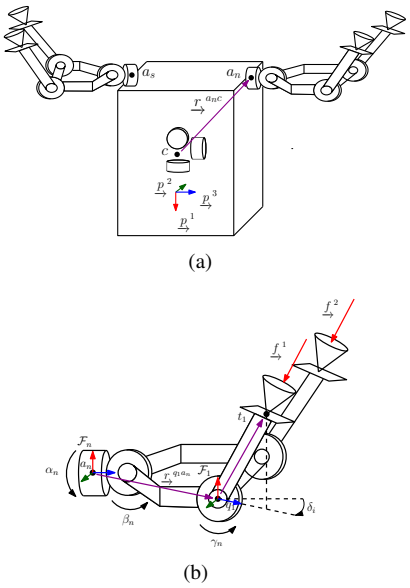

Fig. 1. Schematic adopted from [7] of the (a) spacecraft including three axisymmetric reaction wheels and four electric thrusters, and (b) North-facing boom-thruster assembly. The first, second, and third axes of each reference frame are respectively denoted by red, green, and blue vectors.

the attitude of $\mathcal{F}_b$ relative to $\mathcal{F}_a$. Principle rotations about the $\underrightarrow{a}^{\,i}$ axis by an angle α are denoted as $\mathbf{C}_{ba} = \mathbf{C}_i(\alpha)$. The anti-symmetric projection operator $\boldsymbol{\mathcal{P}}_a(\cdot) : \mathbb{R}^{3\times3} \to \mathfrak{so}(3)$, is given by $\boldsymbol{\mathcal{P}}_a(\mathbf{U}) = \frac{1}{2}\left(\mathbf{U} - \mathbf{U}^{\mathsf{T}}\right)$, for all $\mathbf{U} \in \mathbb{R}^{3\times3}$, where $\mathfrak{so}(3) = \{\mathbf{S} \in \mathbb{R}^{3\times3} \,|\, \mathbf{S} + \mathbf{S}^{\mathsf{T}} = \mathbf{0}\}$. The cross operator, $(\cdot)^{\times} : \mathbb{R}^3 \to \mathfrak{so}(3)$, is defined as $\mathbf{a}^{\times} = -\mathbf{a}^{\times^{\mathsf{T}}} = \begin{bmatrix} 0 & -a_3 & a_2 \\ a_3 & 0 & -a_1 \\ -a_2 & a_1 & 0 \end{bmatrix}$, where $\mathbf{a}^{\mathsf{T}} = \begin{bmatrix} a_1 & a_2 & a_3 \end{bmatrix}$. The uncross operator, $(\cdot)^{\vee} : \mathfrak{so}(3) \to \mathbb{R}^3$, is defined as $\mathbf{A}^{\vee} = \begin{bmatrix} a_1 & a_2 & a_3 \end{bmatrix}^{\mathsf{T}}$, where $\mathbf{A} = \mathbf{a}^{\times}$. The physical vector describing the position of p relative to q is $\underrightarrow{r}^{pq}$. Similarly, the angular velocity of $\mathcal{F}_b$ relative to $\mathcal{F}_a$ is $\underrightarrow{\omega}^{ba}$.

II. Objectives and Spacecraft Model

Consider the satellite shown in Fig. 1, which consists of a rigid bus equipped with three axisymmetric reaction wheels and four electric thrusters mounted on gimbaled booms, which is nominally in a circular GEO orbit. The control objectives are to 1) minimize the effect of quantization on Δv and 2) limit the number of on-off thruster pulses, while ensuring that the satellite is maintained within the prescribed station-keeping window, a nadir-pointing attitude is maintained, angular momentum stored in the reaction wheels is unloaded, and the limitations of the thrusters (e.g., thrust magnitude, boom gimbal angle limits) are enforced. Previous work [7], [8] attempted to minimize fuel consumption using MPC policies. An MPC policy is also adopted in this paper, with a novel quantization scheme that is designed to specifically minimize the effect of quantization on Δv and reduce the number of on-off thruster pulses compared to [7].

The Earth-centered inertial (ECI) frame is defined as $\mathcal{F}_g$. The reference frame $\mathcal{F}_p$ is aligned with the spacecraft bus, where nominally $\underrightarrow{p}^{\,1}$ points towards the Earth and $\underrightarrow{p}^{\,2}$ points North. The angular velocity of $\mathcal{F}_p$ relative to $\mathcal{F}_g$ is $\underrightarrow{\omega}^{pg}$ and the DCM describing the attitude of the spacecraft (i.e., $\mathcal{F}_p$) relative to $\mathcal{F}_g$ is $\mathbf{C}_{pg}$. The spacecraft center of mass is denoted by point c in Fig. 1(a). The position of c relative to a point w at the center of the Earth is given by $\underrightarrow{r}^{cw}$. The equations of motion of the satellite are [7]

$$\ddot{\mathbf{r}}_g^{cw} = -\mu \frac{\mathbf{r}_g^{cw}}{\left\|\mathbf{r}_g^{cw}\right\|^3} + \mathbf{a}_g^p + \frac{1}{m_{\mathcal{B}}} \mathbf{C}_{pg}^{\mathsf{T}} \mathbf{f}_p^{\text{thrust}}, \tag{1a}$$

$$\mathbf{J}_p^{\mathcal{B}c} \dot{\boldsymbol{\omega}}_p^{pg} = -\boldsymbol{\omega}_p^{pg^{\times}} \left(\mathbf{J}_p^{\mathcal{B}c} \boldsymbol{\omega}_p^{pg} + \mathbf{J}_s \dot{\boldsymbol{\gamma}}\right) - \mathbf{J}_s \boldsymbol{\eta} + \boldsymbol{\tau}_p^p + \boldsymbol{\tau}_p^{\text{thrust}}, \tag{1b}$$

$$\dot{\mathbf{C}}_{pg} = -\boldsymbol{\omega}_p^{pg^{\times}} \mathbf{C}_{pg}, \tag{1c}$$

$$\ddot{\boldsymbol{\gamma}} = \boldsymbol{\eta}, \tag{1d}$$

where $m_{\mathcal{B}}$ is the mass of the spacecraft, $\mathbf{J}_p^{\mathcal{B}c}$ is the moment of inertia of the spacecraft relative to point c and resolved in $\mathcal{F}_p$, $\boldsymbol{\gamma}^{\mathsf{T}} = \begin{bmatrix} \gamma_1 & \gamma_2 & \gamma_3 \end{bmatrix}$ are the reaction wheel angles, $\boldsymbol{\eta}$ is the acceleration of the reaction wheels, $\mathbf{J}_s$ is the moment of inertia of the reaction wheel array, $\mathbf{f}_p^{\text{thrust}}$ is the force produced by the thrusters, $\boldsymbol{\tau}_p^{\text{thrust}}$ is the torque produced by the thrusters, $\mathbf{a}_g^p$ includes acceleration perturbations, and $\boldsymbol{\tau}_p^p$ includes torque perturbations. The thruster configuration is illustrated in Fig. 1, where four electric thrusters are mounted on two boom-thruster assemblies, which nominally point North and South, respectively. A detailed view of the North-facing boom-thruster assembly is in Fig. 1(b). Each assembly has two fixed gimbal angles, $\bar{\alpha}_a$ and $\bar{\beta}_a$, $a \in \{n, s\}$, as well as an actuated gimbal angle γ_a, $a \in \{n, s\}$. The subscripts n and s refer to the North- and South-facing assemblies, respectively. The position of the actuated gimbal of thruster i relative to the spacecraft center of mass is $\underrightarrow{r}^{\,q_i c}$. The thrusters are canted by fixed angles δ_i, $i = 1, 2, 3, 4$, such that for $\bar{\gamma}_a$, $a \in \{n, s\}$, each thruster fires through the spacecraft center of mass. The force vector produced by thruster i is $\underrightarrow{f}^{\,i}$, and is resolved in $\mathcal{F}_p$ as $\mathbf{f}_p^i = -f^i \mathbf{C}_{ip}^{\mathsf{T}} \mathbf{C}_2(\gamma_a) \mathbf{1}_3$, where $f^i = \left|\underrightarrow{f}^{\,i}\right|$ is the thrust magnitude, $\mathbf{1}_3 = \begin{bmatrix} 0 & 0 & 1 \end{bmatrix}^{\mathsf{T}}$, $\mathbf{C}_{ip} = \mathbf{C}_{ia}\mathbf{C}_{ap}$, $\mathbf{C}_{ia} = \mathbf{C}_1(\delta_i)\mathbf{C}_2(\bar{\beta}_i)\mathbf{C}_3(\bar{\alpha}_a)$, $\mathbf{C}_{np} = \mathbf{C}_3(\pi)$, and $\mathbf{C}_{sp} = \mathbf{C}_1(\pi)\mathbf{C}_3(\pi)$. The torque generated by the thruster on the spacecraft is $\boldsymbol{\tau}_p^i = \mathbf{r}_p^{q_i c^{\times}} \mathbf{f}_p^i$. The net force and torque of the four thrusters is $\mathbf{f}_p^{\text{thrust}} = \sum_{i=1}^4 \mathbf{B}_i^f \mathbf{u}_i$ and $\boldsymbol{\tau}_p^{\text{thrust}} = \sum_{i=1}^4 \mathbf{B}_i^{\tau} \mathbf{u}_i$, with $\mathbf{u}_i^{\mathsf{T}} = \begin{bmatrix} \sin(\gamma_a) f^i & \cos(\gamma_a) f^i \end{bmatrix}$ and constant input matrices $\mathbf{B}_i^f = \mathbf{C}_{ip}^{\mathsf{T}} \begin{bmatrix} -1 & 0 \\ 0 & 0 \\ 0 & -1 \end{bmatrix}$, $\mathbf{B}_i^{\tau} = \mathbf{r}_p^{q_i c^{\times}} \mathbf{B}_i^f$.

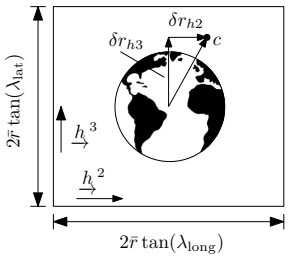

Fig. 2. Illustration of the station keeping window described by $-\bar{r}\tan(\lambda_{\text{long}}) \le \delta r_{h2} \le \bar{r}\tan(\lambda_{\text{long}})$ and $-\bar{r}\tan(\lambda_{\text{lat}}) \le \delta r_{h3} \le \bar{r}\tan(\lambda_{\text{lat}})$, with the view looking in the $-\underrightarrow{h}^{\,1}$ direction towards Earth. The point c denotes the spacecraft's center of mass.

For the purposes of station keeping and linearizing the spacecraft's equations of motion, it is useful to express the spacecraft's position relative to the desired nominal circular GEO orbit. To this end, Hill's frame, $\mathcal{F}_h$, is defined by

basis vectors $\underrightarrow{h}^1$ aligned with the orbital radius and $\underrightarrow{h}^3$ orthogonal to the orbital plane. Resolving $\underrightarrow{r}^{cw}$ in $\mathcal{F}_h$ gives $\mathbf{r}_h^{cw}$. The spacecraft's nominal position in a circular orbit resolved in $\mathcal{F}_g$ is $\bar{\mathbf{r}}_g$, yielding the position error of the spacecraft $\delta\mathbf{r}_h = \begin{bmatrix}\delta r_{h1} & \delta r_{h2} & \delta r_{h3}\end{bmatrix} = \mathbf{r}_h^{cw} - \mathbf{C}_{hg}\bar{\mathbf{r}}_g$. The station keeping window, shown in Fig. 2, is defined as $-\bar{r}\tan(\lambda_{\text{long}}) \leq \delta r_{h2} \leq \bar{r}\tan(\lambda_{\text{long}})$ and $-\bar{r}\tan(\lambda_{\text{lat}}) \leq \delta r_{h3} \leq \bar{r}\tan(\lambda_{\text{lat}})$ [12], where $\bar{r} = \|\bar{\mathbf{r}}_g\|$, and λ_{long}, λ_{lat} are maximum deviations in longitude and latitude, respectively.

III. MPC Formulation

The MPC policy presented in this section is largely based on the MPC policy in [9], with the exception of the positive integer control parameter N_{fb}, which determines the number of time steps between control updates.

A. Inner-Loop Attitude Controller

The reaction wheels are actuated by an attitude controller, which is an inner-loop controller to the MPC policy. The disturbance torque is assumed to be described by the LTI system $\dot{\mathbf{x}}_{\text{dist}} = \mathbf{A}_{\text{dist}}\mathbf{x}_{\text{dist}}$, $\boldsymbol{\tau}_p^p = \mathbf{C}_{\text{dist}}\mathbf{x}_{\text{dist}}$. An observer estimates the disturbance as $\dot{\hat{\mathbf{x}}}_{\text{dist}} = \mathbf{A}_{\text{dist}}\hat{\mathbf{x}}_{\text{dist}} + \mathbf{B}_{\text{dist}}\mathbf{u}_{\text{dist}}$ and $\hat{\boldsymbol{\tau}}_p^p = \mathbf{C}_{\text{dist}}\hat{\mathbf{x}}_{\text{dist}}$, where $\hat{\boldsymbol{\tau}}_p^p$ is the estimate of $\boldsymbol{\tau}_p^p$, $\mathbf{u}_{\text{dist}} = \boldsymbol{\omega}_p^{pd} + \mathbf{K}_1\mathbf{S}$, $\mathbf{K}_1 = \mathbf{K}_1^{\mathsf{T}} > 0$, and $\mathbf{S} = -\boldsymbol{\mathcal{P}}_a\left(\mathbf{C}_{pd}\right)^{\vee}$. The matrix $\mathbf{B}_{\text{dist}} = \mathbf{P}_{\text{dist}}^{-1}\mathbf{C}_{\text{dist}}^{\mathsf{T}}$ is chosen such that $(\mathbf{A}_{\text{dist}}, \mathbf{B}_{\text{dist}}, \mathbf{C}_{\text{dist}})$ is positive real, where $\mathbf{P}_{\text{dist}} = \mathbf{P}_{\text{dist}}^{\mathsf{T}} \geq 0$ satisfies the Lyapunov equation $\mathbf{A}_{\text{dist}}^{\mathsf{T}}\mathbf{P}_{\text{dist}} + \mathbf{P}_{\text{dist}}\mathbf{A}_{\text{dist}} = -\mathbf{Q}_{\text{dist}}$ with $\mathbf{Q}_{\text{dist}} = \mathbf{Q}_{\text{dist}}^{\mathsf{T}} \geq 0$ [13, p. 218]. The attitude controller adapted from [14] is $\boldsymbol{\nu}_1 = \boldsymbol{\omega}_p^{\times}\left(\mathbf{J}_p^{\mathcal{B}c}\boldsymbol{\omega}_p + \mathbf{J}_s\dot{\boldsymbol{\gamma}}\right) - \mathbf{J}_p^{\mathcal{B}c}\left(\mathbf{K}_1\dot{\mathbf{S}} + \boldsymbol{\omega}_p^{pd\times}\boldsymbol{\omega}_p\right)$, $\boldsymbol{\nu}_2 = -\hat{\boldsymbol{\tau}}_p^p$, $\boldsymbol{\nu}_3 = -\mathbf{K}_{\nu}\left(\boldsymbol{\omega}_p^{pd} + \mathbf{K}_1\mathbf{S}\right) - \mathbf{K}_p\mathbf{S}$, where $\mathbf{K}_{\nu} = \mathbf{K}_{\nu}^{\mathsf{T}} > 0$, $\mathbf{K}_p = \mathbf{K}_p^{\mathsf{T}} > 0$, and the control input is $\boldsymbol{\eta} = -\mathbf{J}_s^{-1}\left(\boldsymbol{\nu}_1 + \boldsymbol{\nu}_2 + \boldsymbol{\nu}_3\right)$.

B. Closed-Loop Linearized Model

The MPC prediction model is obtained by linearizing the spacecraft dynamics in closed-loop with the attitude controller about a nominal circular orbit with mean motion n, a nadir-pointing attitude, zero reaction wheel speeds, and zero observer states, and is given by $\delta\ddot{\mathbf{r}}_h = -2\bar{\boldsymbol{\omega}}_p^{\times}\delta\dot{\mathbf{r}}_h - \boldsymbol{\Omega}\delta\mathbf{r}_h + \mathbf{a}_h^p + \frac{1}{m_{\mathcal{B}}}\mathbf{C}_{dh}^{\mathsf{T}}\mathbf{f}_p^{\text{thrust}}$, $\delta\dot{\boldsymbol{\omega}} = \left(\mathbf{K}_1\bar{\boldsymbol{\omega}}_p^{\times} - \left(\bar{\boldsymbol{\omega}}_p^{\times}\right)^2 + \mathbf{J}_p^{\mathcal{B}c^{-1}}\left(\mathbf{K}_{\nu}\bar{\boldsymbol{\omega}}_p^{\times} - \mathbf{K}\right)\right)\delta\boldsymbol{\theta} + \boldsymbol{\tau}_p^{\text{thrust}} + \left(-\mathbf{K}_1 + \bar{\boldsymbol{\omega}}_p^{\times} - \mathbf{J}_p^{\mathcal{B}c}\mathbf{K}_{\nu}\right)\delta\boldsymbol{\omega} - \mathbf{J}_p^{\mathcal{B}c^{-1}}\mathbf{C}_{\text{dist}}\tilde{\mathbf{x}}_{\text{dist}}$, $\ddot{\boldsymbol{\gamma}} = \boldsymbol{\eta}$, $\dot{\tilde{\mathbf{x}}} = \mathbf{A}_{\text{dist}}\tilde{\mathbf{x}}_{\text{dist}} + \mathbf{B}_{\text{dist}}\delta\boldsymbol{\omega} + \mathbf{B}_{\text{dist}}\left(\mathbf{K}_1 - \bar{\boldsymbol{\omega}}_p^{\times}\right)\delta\boldsymbol{\theta}$ [7], where $\bar{\boldsymbol{\omega}}_p^{\mathsf{T}} = \begin{bmatrix}0 & 0 & n\end{bmatrix}$, $\mathbf{C}_{pd} = \mathbf{C}_{pg}\mathbf{C}_{dg}^{\mathsf{T}}$ is the attitude error between $\mathbf{C}_{pg}$ and the desired nadir-pointing orientation $\mathbf{C}_{dg}$, $\mathbf{C}_{pg}$ is parameterized by a 3-2-1 Euler angle sequence with angles $\delta\boldsymbol{\theta}^{\mathsf{T}} = \begin{bmatrix}\delta\phi & \delta\theta & \delta\psi\end{bmatrix}$, $\mathbf{K} = \mathbf{K}_{\nu}\mathbf{K}_1 + \mathbf{K}_p$, and $\boldsymbol{\Omega} = \text{diag}\{-3n^2, 0, n^2\}$. The closed-loop linearized model in state-space form is $\dot{\mathbf{x}} = \mathbf{A}\mathbf{x} + \mathbf{B}\mathbf{u} + \mathbf{B}_w\mathbf{w}$, where $\mathbf{x}^{\mathsf{T}} = \begin{bmatrix}\delta\mathbf{r}^{\mathsf{T}} & \delta\dot{\mathbf{r}}^{\mathsf{T}} & \delta\boldsymbol{\theta}^{\mathsf{T}} & \delta\boldsymbol{\omega}^{\mathsf{T}} & \dot{\boldsymbol{\gamma}}^{\mathsf{T}} & \tilde{\mathbf{x}}_{\text{dist}}^{\mathsf{T}}\end{bmatrix}$, $\mathbf{u}^{\mathsf{T}} = \begin{bmatrix}\mathbf{u}_1^{\mathsf{T}} & \mathbf{u}_2^{\mathsf{T}} & \mathbf{u}_3^{\mathsf{T}} & \mathbf{u}_4^{\mathsf{T}}\end{bmatrix}$, and $\mathbf{w} = \mathbf{a}_h^p$. The discrete-time model with time step Δt is $\mathbf{x}_{k+1} = \mathbf{A}_{\text{d}}\mathbf{x}_k + \mathbf{B}_{\text{d}}\mathbf{u}_k + \mathbf{B}_{w,\text{d}}\mathbf{w}_k$.

C. MPC Input and State Constraints

The magnitude of each thruster must satisfy $\left\|\mathbf{f}_i^i\right\|_2 \leq f_{\text{max}}$, where f_{max} is the maximum allowable thrust. To simplify the MPC formulation, this quadratic constraint is approximated by the linear constraint $\left\|\mathbf{f}_i^i\right\|_1 \leq f_{\text{max}}$. It is also imperative that the thrusters fire away from the spacecraft bus, which is enforced by the constraint $\mathbf{f}_i^i \leq 0$. The control constraints are $\mathbf{u}_{\text{min}} \leq \mathbf{u}_i \leq \mathbf{u}_{\text{max}}$, $i = 1, 2, 3, 4$, where $\mathbf{u}_{\text{max}}^{\mathsf{T}} = f_{\text{max}}\begin{bmatrix}1 & 1\end{bmatrix}$ and $\mathbf{u}_{\text{min}} = \mathbf{0}$. There is an additional physical constraint that the gimbal angle γ_n must be identical for the pair of inputs $\mathbf{u}_1$ and $\mathbf{u}_2$ at any time instant, since they share this angle. The same is true for γ_s with the pair of inputs $\mathbf{u}_3$ and $\mathbf{u}_4$. As in [7], this constraint is ignored in the MPC policy and is addressed in the quantization scheme. The state constraints considered in this policy are based on the prescribed station keeping window and the maximum allowable attitude error. Since the closed-loop linearized orbital dynamics equation of motion is given in Hill's frame, the station keeping window constraint is $\delta\bar{\mathbf{r}}_{\text{min}} \leq \delta\bar{\mathbf{r}} \leq \delta\bar{\mathbf{r}}_{\text{max}}$, where $\delta\bar{\mathbf{r}}_{\text{max}}^{\mathsf{T}} = \begin{bmatrix}\infty & \bar{r}\tan(\lambda_{\text{long}}) & \bar{r}\tan(\lambda_{\text{lat}})\end{bmatrix}$, and $\delta\bar{\mathbf{r}}_{\text{min}} = -\delta\bar{\mathbf{r}}_{\text{max}}$. The constraint on attitude error is $\delta\boldsymbol{\theta}_{\text{min}} \leq \delta\boldsymbol{\theta} \leq \delta\boldsymbol{\theta}_{\text{max}}$.

D. MPC Policy

Consider the split-horizon MPC policy [9] stated as

$$\min_{\mathcal{U}_t} \ \mathbf{x}_{N_1|t}^{\mathsf{T}}\mathbf{P}_1\mathbf{x}_{N_1|t} + \sum_{k=0}^{N_1-1}\left(\mathbf{x}_{k|t}^{\mathsf{T}}\mathbf{Q}\mathbf{x}_{k|t} + \mathbf{u}_{k|t}^{\mathsf{T}}\mathbf{R}\mathbf{u}_{k|t}\right) + \mathbf{x}_{N_2|t}^{\mathsf{T}}\mathbf{P}_2\mathbf{x}_{N_2|t} + \sum_{k=N_1}^{N_2-1}\left(\mathbf{x}_{k|t}^{\mathsf{T}}\mathbf{Q}_2\mathbf{x}_{k|t} + \mathbf{u}_{k|t}^{\mathsf{T}}\mathbf{R}\mathbf{u}_{k|t}\right), \quad (2)$$

subject to $\mathbf{x}_{k+1|t} = \mathbf{A}_{\text{d}}\mathbf{x}_{k|t} + \mathbf{B}_{\text{d}}\mathbf{u}_{k|t} + \mathbf{B}_{w,\text{d}}\mathbf{w}_{k|t}$, $\mathbf{x}_{0|t} = \mathbf{x}(t)$, $\mathbf{w}_{k|t} = \hat{\mathbf{w}}_t(t+k)$, $\mathbf{x}_{\text{min}} \leq \mathbf{x}_{k|t} \leq \mathbf{x}_{\text{max}}$ for $0 \leq k \leq N_1$, $\mathbf{x}_{\text{min},2} \leq \mathbf{x}_{k|t} \leq \mathbf{x}_{\text{max},2}$ for $N_1 < k \leq N_2$, and $\mathbf{u}_{\text{min}} \leq \mathbf{u}_{k|t} \leq \mathbf{u}_{\text{max}}$, where N_1 is the prediction horizon of the states δr_{h3}^{cw} and $\delta\dot{r}_{h3}^{cw}$, N_2 is the prediction horizon of the remaining states, $\mathcal{U}_t = \{\mathbf{u}_{0|t}, \ldots, \mathbf{u}_{N_2-1|t}\}$, $\mathbf{Q} = \mathbf{Q}^{\mathsf{T}} \geq 0$ and $\mathbf{R} = \mathbf{R}^{\mathsf{T}} > 0$ are constant state and control weighting matrices, and $\hat{\mathbf{w}}_i(j)$ is the open-loop predicted disturbance column matrix at time j based on data at time i. The matrix $\mathbf{Q}_2$ is the same as $\mathbf{Q}$, except the rows and columns associated with the states δr_{h3}^{cw} and $\delta\dot{r}_{h3}^{cw}$ are set to zero. The matrices $\mathbf{P}_1$ and $\mathbf{P}_2$ are constructed from the matrix $\mathbf{P} = \mathbf{P}^{\mathsf{T}} > 0$, which is the solution to the Discrete Algebraic Riccati Equation (DARE). The matrix $\mathbf{P}_1$ contains the rows and columns of $\mathbf{P}$ associated with the states δr_{h3}^{cw} and $\delta\dot{r}_{h3}^{cw}$ and zeros the others, while $\mathbf{P}_2$ does the opposite, so that $\mathbf{P}_1 + \mathbf{P}_2 = \mathbf{P}$. This is possible since $\mathbf{P}$ is block-diagonal under a coordinate transformation that reorders the states such that δr_{h3}^{cw} and $\delta\dot{r}_{h3}^{cw}$ are at the end of the state column matrix. The state constraints $\mathbf{x}_{\text{min}}$ and $\mathbf{x}_{\text{max}}$ are based on the station keeping and attitude constraints. The state constraints $\mathbf{x}_{\text{min},2}$ and $\mathbf{x}_{\text{max},2}$ are identical to $\mathbf{x}_{\text{min}}$ and $\mathbf{x}_{\text{max}}$, except $\delta\mathbf{r}_{\text{min}}^{\mathsf{T}} = \begin{bmatrix}-\infty & -\bar{r}\tan(\lambda_{\text{long}}) & -\infty\end{bmatrix}$ and $\delta\mathbf{r}_{\text{max}}^{\mathsf{T}} = \begin{bmatrix}\infty & \bar{r}\tan(\lambda_{\text{long}}) & \infty\end{bmatrix}$ are used. The control input sequence is $\mathbf{u}(t+j) = \mathbf{u}_{j|t}^*$, $j = 0, \ldots, N_{\text{fb}} - 1$, where $\mathcal{U}_t^*$ is the minimizer of (2), and N_{fb} is the number of time steps between control updates.

IV. Single-Pulse Quantization Scheme

The low-thrust electric thrusters considered for this spacecraft are operated with on-off pulses. The control input generated by the MPC policy described in Section III-D is

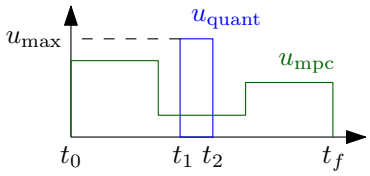

Fig. 3. Single quantized on-off thrust pulse (u_{quant}) over one feedback period with three discrete time steps ($N_{\text{fb}} = 3$) for a given thruster.

a continuous thrust value for each thruster, which cannot be used directly with on-off thrusters, or in the propulsion system assembly shown in Fig. 1. As such, the control input must be quantized to on-off pulses that satisfy the physical constraints of the thrusters and the propulsion system assembly. A PWM quantization scheme is developed in [7] with a fixed frequency of five on-off pulses per time step with varying pulse widths such that the average thrust matched the constant thrust of the MPC control input over each time step. This works well, but leads to a large number of on-off pulses, on the order of 30 pulses per thruster per orbit. To reduce the number of on-off pulses, a single pulse quantization scheme over a feedback period is proposed in this section.

As shown in Fig. 3, consider the quantization of a piecewise constant control input sequence, $\mathbf{u}_{\text{mpc}}$, over a time step beginning at time t_0 and ending at time $t_f = t_0 + N_{\text{fb}}\Delta t$, where only a single pulse of magnitude $f_{\max}$ is applied at the i^{th} thruster starting at time $t_{1,i}$ and ending at time $t_{2,i}$, and $t_0 \leq t_{1,i} < t_{2,i} \leq t_f$. The thruster on and off times are solved such that $\mathbf{e}^{\mathsf{T}}\mathbf{W}\mathbf{e}$ is minimized, where $\mathbf{e} = \mathbf{x}_{\text{mpc}}(t_f) - \mathbf{x}_{\text{quant}}(t_f)$; $\mathbf{x}_{\text{mpc}}(t_f)$ and $\mathbf{x}_{\text{quant}}(t_f)$ are the predicted states at t_f using the MPC input sequence $\mathbf{u}_{\text{mpc}}$ and the quantized inputs, respectively; $\mathbf{W} = \mathbf{W}^{\mathsf{T}} \geq 0$ is a weighting matrix; and the variable $N_{\text{fb}} \in \mathbb{Z}^+$ is the number of discretization time steps in a feedback period.

The predicted states of the system at time t_f based on the quantized thrust inputs are given by $\mathbf{x}_{\text{quant}}(t_f) = e^{\mathbf{A}N_{\text{fb}}\Delta t}\mathbf{x}(t_0) + \sum_{i=1}^{4} e^{\mathbf{A}(t_f - t_{2,i})}\mathbf{B}_{d,i}(t_{1,i}, t_{2,i})\mathbf{u}_{\max,i}$, where

$$\mathbf{u}_{\max,i} = \begin{cases} f_{\max}\dfrac{\bar{\mathbf{u}}_{\text{mpc},t_0,i}}{\left\|\bar{\mathbf{u}}_{\text{mpc},j|t_0,i}\right\|} & \left\|\bar{\mathbf{u}}_{\text{mpc},t_0,i}\right\| \geq N_{\text{fb}}\epsilon \\ \mathbf{0} & \left\|\bar{\mathbf{u}}_{\text{mpc},t_0,i}\right\| < N_{\text{fb}}\epsilon \end{cases},$$

$\bar{\mathbf{u}}_{\text{mpc},t_0,i} = \sum_{j=0}^{N_{\text{fb}}-1} \mathbf{u}_{\text{mpc},j|t_0,i}$, $\mathbf{u}_{\text{mpc},j|t_0}^{\mathsf{T}} = \begin{bmatrix}\mathbf{u}_{\text{mpc},j|t_0,1}^{\mathsf{T}} & \mathbf{u}_{\text{mpc},j|t_0,2}^{\mathsf{T}} & \mathbf{u}_{\text{mpc},j|t_0,3}^{\mathsf{T}} & \mathbf{u}_{\text{mpc},j|t_0,4}^{\mathsf{T}}\end{bmatrix}$, and $\epsilon > 0$ is the tolerance below which the MPC input is considered to be zero. The calculation of $\mathbf{u}_{\max,i}$ involves averaging the MPC inputs of the i^{th} thruster over the feedback period, which gives a single gimbal angle for each thruster within the feedback period. The predicted states of the system evolution based on the MPC inputs can be expressed as $\mathbf{x}_{\text{mpc}}(t_f) = e^{\mathbf{A}N_{\text{fb}}\Delta t}\mathbf{x}(t_0) + \int_{t_0}^{t_f} e^{\mathbf{A}(t_f-\tau)}\mathbf{B}\mathbf{u}_{\text{mpc}}(\tau)\mathrm{d}\tau = e^{\mathbf{A}N_{\text{fb}}\Delta t}\mathbf{x}(t_0) + \mathbf{C}_{N_{\text{fb}}-1}\mathbf{u}_{\text{mpc},0:N_{\text{fb}}-1|t_0}$, where $\mathbf{C}_{N_{\text{fb}}-1} = \begin{bmatrix}\mathbf{A}_{\text{d}}^{N_{\text{fb}}-1}\mathbf{B}_{\text{d}} & \cdots & \mathbf{A}_{\text{d}}\mathbf{B}_{\text{d}} & \mathbf{B}_{\text{d}}\end{bmatrix}$ is the controllability matrix, $\mathbf{A}_{\text{d}} = e^{\mathbf{A}\Delta t}\mathbf{x}(t_0)$ is the discrete-time $\mathbf{A}$ matrix calculated with time step Δt, $\mathbf{B}_{\text{d}} = \int_0^{\Delta t} e^{\mathbf{A}(\Delta t-\tau)}\mathrm{d}\tau\mathbf{B}$ is the discrete-time $\mathbf{B}$ matrix calculated with time step Δt, and $\mathbf{u}_{\text{mpc},0:N_{\text{fb}}-1|t_0}^{\mathsf{T}} = \begin{bmatrix}\mathbf{u}_{\text{mpc},0|t_0}^{\mathsf{T}} & \cdots & \mathbf{u}_{\text{mpc},N_{\text{fb}}-2|t_0}^{\mathsf{T}} & \mathbf{u}_{\text{mpc},N_{\text{fb}}-1|t_0}^{\mathsf{T}}\end{bmatrix}$. The error between the two predicted states at t_f is given by $\mathbf{e} = \mathbf{x}_{\text{mpc}}(t_f) - \mathbf{x}_{\text{quant}}(t_f) = \mathbf{C}_{N_{\text{fb}}-1}\mathbf{u}_{\text{mpc},0:N_{\text{fb}}-1|t_0} - \sum_{i=1}^{4} e^{\mathbf{A}(t_f-t_{2,i})}\mathbf{B}_{d,i}(t_{1,i}, t_{2,i})\mathbf{u}_{\max,i}$. The switching times for each thruster must satisfy $t_0 \leq t_{1,i} < t_{2,i} \leq t_f$, $i = 1, 2, 3, 4$. Additionally, not more than one thruster on either boom-thruster assembly should fire at a given time, since these thrusters share the gimbal angle γ_a, $a \in \{n, s\}$, and hence their directions cannot differ. This constrains the switching times of the thrusters to not overlap. As the firing order of the thrusters may have an impact on the predicted state error, different orders of thruster firings are considered: 1 before 2 and 3 before 4 (Mode 1), as well as 2 before 1 and 4 before 3 (Mode 2). Defining the design variable $\mathbf{t}^{\mathsf{T}} = \begin{bmatrix}t_{1,1} & t_{2,1} & t_{1,2} & t_{2,2} & t_{1,3} & t_{2,3} & t_{1,4} & t_{2,4}\end{bmatrix}$, the thruster switching constraints are $\mathbf{A}_{t,i}\mathbf{t} \leq \mathbf{b}_{t,i}$, $i = 1, 2$, where $\mathbf{b}_{t,i}^{\mathsf{T}} = \begin{bmatrix}0 & 0 & 0 & 0 & -t_0 & t_f & -t_0 & t_f & 0 & 0\end{bmatrix}$,

$$\mathbf{A}_{t,i} = \begin{bmatrix}\mathbf{A}_t \\ \bar{\mathbf{A}}_{t,i}\end{bmatrix},\ \mathbf{A}_t = \begin{bmatrix}1 & -1 & 0 & 0 & 0 & 0 & 0 & 0 \\ 0 & 0 & 1 & -1 & 0 & 0 & 0 & 0 \\ 0 & 0 & 0 & 0 & 1 & -1 & 0 & 0 \\ 0 & 0 & 0 & 0 & 0 & 0 & 1 & -1\end{bmatrix},$$

and the contents of $\bar{\mathbf{A}}_{t,i}$ depend on the thruster-firing mode considered. The matrix $\mathbf{A}_t$ and the first four rows of $\mathbf{b}_{t,i}$ ensure that $t_{1,i} \leq t_{2,i}$, while $\bar{\mathbf{A}}_{t,i}$ and the last six rows of $\mathbf{b}_{t,i}$ determine the thruster firing order. The contents of $\bar{\mathbf{A}}_{t,i}$ for Modes 1 and 2, respectively, are

$$\bar{\mathbf{A}}_{t,1} = \begin{bmatrix}-1 & 0 & 0 & 0 & 0 & 0 & 0 & 0 \\ 0 & 0 & 0 & 1 & 0 & 0 & 0 & 0 \\ 0 & 0 & 0 & 0 & -1 & 0 & 0 & 0 \\ 0 & 0 & 0 & 0 & 0 & 0 & 0 & 1 \\ 0 & 1 & -1 & 0 & 0 & 0 & 0 & 0 \\ 0 & 0 & 0 & 0 & 0 & 1 & -1 & 0\end{bmatrix},$$

$$\bar{\mathbf{A}}_{t,2} = \begin{bmatrix}0 & 0 & -1 & 0 & 0 & 0 & 0 & 0 \\ 0 & 1 & 0 & 0 & 0 & 0 & 0 & 0 \\ 0 & 0 & 0 & 0 & 0 & 0 & -1 & 0 \\ 0 & 0 & 0 & 0 & 0 & 1 & 0 & 0 \\ -1 & 0 & 0 & 1 & 0 & 0 & 0 & 0 \\ 0 & 0 & 0 & 0 & -1 & 0 & 0 & 1\end{bmatrix}.$$

If no thrusters are on during the feedback period, then all thrust commands are set to zero for the entire period and no optimization problem is solved. Otherwise, the optimization problem to be solved is $\min_{t_{1,i},\, t_{2,i},\ i=1,2,3,4} \mathbf{e}^{\mathsf{T}}\mathbf{W}\mathbf{e}$, subject to $\mathbf{A}_{t,1}\mathbf{t} \leq \mathbf{b}_{t,1}$. The optimization problem is solved again with the constraint $\mathbf{A}_{t,2}\mathbf{t} \leq \mathbf{b}_{t,2}$. The solution that results in a smaller cost function value is used as the optimal solution. In practice, it is observed that a suitable value of $\mathbf{W}$ is one that normalizes the magnitudes of the states, thus providing equal importance to the error in the different states.

V. Numerical Simulation Analysis

The quantization scheme and MPC policy in Sections III and IV are implemented in a numerical simulation of the nonlinear spacecraft dynamic model presented in (1), which has been validated using Systems Tool Kit (STK) in [8]. A spacecraft in GEO is considered using the same physical parameters as [7]. The spacecraft has a mass of 4000 kg, and reactions wheels each with a mass of 20 kg, a radius of 0.75 m, and a thickness of 0.2 m. The nominal gimbal angles of the boom-thruster assemblies are $\bar{\alpha}_n = \bar{\alpha}_s = \bar{\beta}_n = \bar{\beta}_s = 0°$ and $\bar{\gamma}_n = \bar{\gamma}_s = 40.14°$. Further details of the boom-thruster assembly physical parameters can be found in [7]. Perturbations due to Earth's oblateness, solar

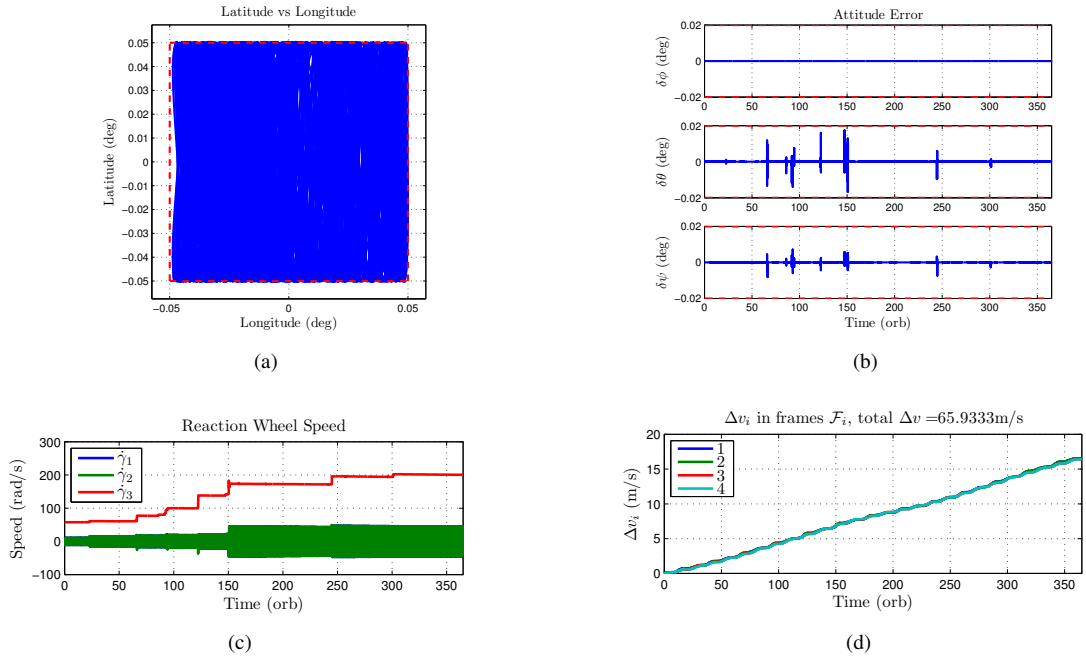

Fig. 4. One year simulation using the quantized MPC policy of Section III. Plots include the (a) station keeping window, (b) spacecraft attitude error, (c) reaction wheel speeds, and (d) accumulation of Δv for each thruster.

and lunar gravitational attraction, and solar radiation pressure are included in the simulation [8]. Solar radiation pressure is also considered in the calculation of a disturbance torque, as done in [15, p. 229], with the numerical values found in [7]. The performance constraints considered in simulation include a maximum thruster magnitude of 0.1 N, a station keeping window of $\pm 0.05^\circ$ in both latitude and longitude, and a maximum allowable attitude error of $\pm 0.02^\circ$ in yaw, pitch, and roll. Simulations are performed for 425 orbits, but only the results from the last 365 orbits are presented and used for analysis, to remove the initial transient behavior.

The MPC policy uses a split prediction horizon of $N_1 = 5$ hours, $N_2 = 20$ hours, a discretization time step of $\Delta t = 1$ hour, and weighting matrices of $\mathbf{Q} = \text{diag}\{\mathbf{Q}_\mathbf{r}, \mathbf{Q}_{\dot{\mathbf{r}}}, \mathbf{Q}_{\boldsymbol{\theta}}, \mathbf{Q}_{\boldsymbol{\omega}}, \mathbf{Q}_{\dot{\boldsymbol{\gamma}}}, \mathbf{Q}_{\tilde{\mathbf{x}}_{\text{dist}}}\}$ and $\mathbf{R} = \mathbf{R}_{\text{thrust}} + \mathbf{R}_{\text{torque}}$, where $\mathbf{Q}_\mathbf{r} = 10^{-3} \cdot \text{diag}\{0, 1, 1\}$ 1/m^2, $\mathbf{Q}_{\dot{\mathbf{r}}} = \mathbf{0}$ s^2/m^2, $\mathbf{Q}_{\boldsymbol{\theta}} = 10^{-3} \cdot \mathbf{1}$ 1/rad^2, $\mathbf{Q}_{\boldsymbol{\omega}} = 10^{-3} \cdot \mathbf{1}$ s^2/rad^2, $\mathbf{Q}_{\dot{\boldsymbol{\gamma}}} = 10^{-4} \cdot \mathbf{1}$ s^2/rad^2, $\mathbf{Q}_{\tilde{\mathbf{x}}_{\text{dist}}} = \mathbf{0}$, $\mathbf{R}_{\text{thrust}} = 10^4$ 1/N^2, $\mathbf{R}_{\text{torque}} = 10^4 \cdot \mathbf{L}^\mathsf{T}\mathbf{L}$, where $\mathbf{L} = \text{diag}\{\mathbf{B}_1^\tau, \mathbf{B}_2^\tau, \mathbf{B}_3^\tau, \mathbf{B}_4^\tau\}$. The inner-loop attitude controller gains are $\mathbf{K}_1 = 0.2 \cdot \mathbf{1}$ s^{-1}, $\mathbf{K}_p = 2 \cdot \mathbf{1}$ N·m, $\mathbf{K}_\nu = 100 \cdot \mathbf{1}$ N·m·s. The observer dynamics of the inner-loop attitude controller are chosen as $\mathbf{A}_{\text{dist}} = \text{diag}\{\bar{\mathbf{A}}_{\text{dist}}, \bar{\mathbf{A}}_{\text{dist}}, \bar{\mathbf{A}}_{\text{dist}}\}$ and $\mathbf{C}_{\text{dist}} = \text{diag}\{\bar{\mathbf{C}}_{\text{dist}}, \bar{\mathbf{C}}_{\text{dist}}, \bar{\mathbf{C}}_{\text{dist}}\}$, where $\bar{\mathbf{A}}_{\text{dist}} = \begin{bmatrix} -0.001 & -\omega_d^2 \\ 1 & -0.001 \end{bmatrix}$, $\omega_d = 2\pi$ rad/day, and $\bar{\mathbf{C}}_{\text{dist}} = \begin{bmatrix} 1 & 0 \end{bmatrix}$. The observer matrix $\bar{\mathbf{B}}_{\text{dist}}$ is given by $\bar{\mathbf{B}}_{\text{dist}} = \mathbf{P}_{\text{dist}}^{-1}\bar{\mathbf{C}}_{\text{dist}}^\mathsf{T}$, where $\mathbf{P}_{\text{dist}} = \mathbf{P}_{\text{dist}}^\mathsf{T} \geq 0$ satisfies the Lyapunov equation $\bar{\mathbf{A}}_{\text{dist}}^\mathsf{T}\mathbf{P}_{\text{dist}} + \mathbf{P}_{\text{dist}}\bar{\mathbf{A}}_{\text{dist}} = -\mathbf{Q}_{\text{dist}}$ with $\mathbf{Q}_{\text{dist}} = 10^{-3} \cdot \mathbf{1}$. A simulation is first performed without quantization, which yields $\Delta v = 65.925$ m/s. The single-pulse quantization scheme is then implemented with identical parameters and also a $N_{\text{fb}} = 1$ time step between feedback, a thrust cutoff of $\epsilon = 0.01$ mN, and the weighting matrix $\mathbf{W} = \text{diag}\{\mathbf{W}_\mathbf{r}, \mathbf{W}_{\dot{\mathbf{r}}}, \mathbf{W}_{\boldsymbol{\theta}}, \mathbf{W}_{\boldsymbol{\omega}}, \mathbf{W}_{\dot{\boldsymbol{\gamma}}}, \mathbf{W}_{\tilde{\mathbf{x}}_{\text{dist}}}\}$, where $\mathbf{W}_\mathbf{r} = 10^{-4} \cdot \text{diag}\{1, 1, 10^3\}$ 1/m^2, $\mathbf{W}_{\dot{\mathbf{r}}} = \mathbf{1}$ s^2/m^2, $\mathbf{W}_{\boldsymbol{\theta}} = 10^4 \cdot \mathbf{1}$ 1/rad^2, $\mathbf{W}_{\boldsymbol{\omega}} = 10^{-1} \cdot \mathbf{1}$ s^2/rad^2, $\mathbf{W}_{\dot{\boldsymbol{\gamma}}} = 10 \cdot \mathbf{1}$ s^2/rad^2, and $\mathbf{W}_{\tilde{\mathbf{x}}_{\text{dist}}} = 10 \cdot \mathbf{1}$. The results of this simulation are included in Fig. 4, where a Δv of 65.933 m/s is achieved with an average of 2.7 pulses per thruster per orbit. The number of thruster pulses is reduced by a factor of ten compared to the PWM scheme in [7] and Δv is within 0.01 m/s of the non-quantized result, which highlights the effectiveness of the single-pulse quantization scheme. Figs. 4(a) and 4(b) show that state constraints are satisfied throughout the simulation.

A. Analysis of Quantization Scheme

Numerical simulations are performed to analyze the choice of parameters in the single-pulse quantization scheme. The parameters considered include the thrust cutoff value (ϵ), the number of time steps between feedback (N_{fb}), and the weighting matrix in the quantization objective function ($\mathbf{W}$).

1) Thrust Cutoff Value (ϵ): The thrust cutoff value determines the smallest thrust magnitude to quantize as an on-off thruster pulse. A lower bound on ϵ may be determined by the specifications of the thruster, as on-off electric thrusters often have a minimum pulse width. However, using the lowest possible value of ϵ may not yield the best Δv performance and/or a reasonable number of thruster pulses. Simulations are performed with cutoff values in the range $0.001 \text{ mN} \leq \epsilon \leq 1$ mN to quantify the effect of ϵ on performance, with results shown in Fig. 5. Fig. 5 shows that the relationships between ϵ and the performance metrics Δv and the number of on-off pulses per thruster per orbit is non-trivial. A small value of ϵ can yield reasonable Δv, but results in many thruster pulses (e.g., $\Delta v = 69.6$ m/s and 14.73 pulses/thruster/orbit for $\epsilon = 0.001$ mN). A large value of ϵ typically results in a lower number of thruster pulses, but a large Δv (e.g., $\Delta v = 83.8$ m/s and 5.62 pulses/thruster/orbit

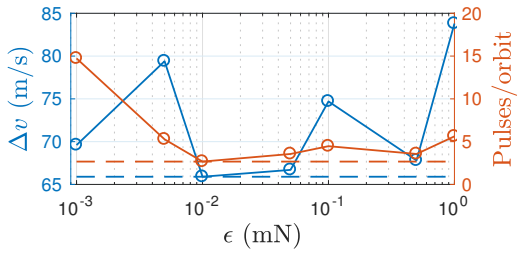

Fig. 5. Effect on Δv and number of thruster pulses/orbit with varying ϵ in quantization scheme. The dashed lines indicate the baseline result.

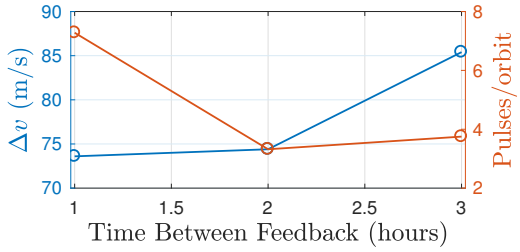

Fig. 6. Effect on Δv and number of thruster pulses/orbit with varying N_{fb} in quantization scheme.

for $\epsilon = 1$ mN). The choice of ϵ ultimately depends on the problem at hand, and is an important tuning parameter in obtaining optimal performance. In our simulations, the optimum is achieved by an intermediate value ($\epsilon = 0.01$ mN).

2) Number of Time Steps Between Feedback (N_{fb}): A feature of the proposed quantization scheme is that a single pulse can be generated for a feedback period that spans more than one discrete time step. The number of time steps between feedback periods is determined by the positive integer parameter N_{fb}. It is observed in simulation that there is an upper bound on N_{fb} determined by the controller parameters, beyond which the error induced by quantization becomes too large to satisfy state constraints. For the controller parameters used in Section V with a split horizon of $N_1 = 5$ hours and $N_2 = 20$ hours, only $N_{\text{fb}} = 1$ is feasible. Therefore, to illustrate the effect of N_{fb} on performance, simulations are performed with a non-split horizon of $N_1 = N_2 = 20$ hours with $N_{\text{fb}} = 1$, $N_{\text{fb}} = 2$, and $N_{\text{fb}} = 3$. The results in Fig. 6 demonstrate how using $N_{\text{fb}} = 2$ instead of $N_{\text{fb}} = 1$ reduces the number of pulses from 7.28 pulses/thruster/orbit to 3.32 pulses/thruster/orbit, but increases Δv from 73.6 m/s to 74.4 m/s. The selection of $N_{\text{fb}} = 3$ yields an increase of both Δv and the number of thruster pulses compared to $N_{\text{fb}} = 2$. As demonstrated, tuning N_{fb} typically allows for a tradeoff in Δv and the number of thruster pulses, but this tuning may be restricted depending on the problem at hand.

3) Weighting Matrix ($\mathbf{W}$): The selection of the weighting matrix in the objective function of the quantization scheme has a significant influence on the quantization results, as the value of $\mathbf{W}$ dictates which state errors to minimize during quantization. Three different choices of $\mathbf{W}$ are examined in this section: $\mathbf{W}_1 = \mathbf{W}$ used in Section V, $\mathbf{W}_2 = \mathbf{W}_1^{1/2}$, and $\mathbf{W} = \mathbf{1}$. Results with $\mathbf{W}_1$, $\mathbf{W}_2$, and $\mathbf{W}_3$ are given in Table I, where $\mathbf{W}_1$ gives the lowest Δv and number of thruster pulses. Based on the authors' experience, it is beneficial to use a weighting matrix that normalizes the states to roughly the same order of magnitude, which is how $\mathbf{W}_1$ was chosen.

TABLE I

EFFECT OF VARYING $\mathbf{W}$ IN QUANTIZATION SCHEME

$\mathbf{W}$	Δv (m/s)	Pulses/orbit
$\mathbf{W}_1$ (Baseline)	65.9	2.67
$\mathbf{W}_2$	75.5	5.27
$\mathbf{W}_3$	66.9	3.65

VI. CONCLUSIONS

This paper presented a novel quantization scheme for the simultaneous station keeping, attitude control, and momentum management of a GEO satellite that yields very little change in performance due to quantization with an order of magnitude less on-off thruster pulses than PWM quantization. The number of on-off thruster pulses obtained is implementable over a 15 year lifespan using existing low-thrust electric propulsion technology. The proposed single-pulse quantization scheme may be applicable to other control problems where quantization of continuous control inputs with a limited number of on-off control inputs is desired.

REFERENCES

[1] M. Martinez-Sanchez and J. E. Pollard, "Spacecraft electric propulsion – an overview," *J. Propul. Power*, vol. 14, no. 5, pp. 688–699, 1998.

[2] A. Sukhanov and A. Prado, "On one approach to the optimization of low-thrust station keeping manoeuvres," *Adv. Apace Res.*, vol. 50, no. 11, pp. 1478 – 1488, 2012.

[3] M. Leomanni, A. Garulli, A. Giannitrapani, and F. Scortecci, "All-electric spacecraft precision pointing using model predictive control," *J. Guid. Control Dynam.*, vol. 38, no. 1, pp. 161–168, 2015.

[4] M. Leomanni, E. Rogers, and S. B. Gabriel, "Explicit model predictive control approach for low-thrust spacecraft proximity operations," *J. Guid. Control Dynam.*, vol. 37, no. 6, pp. 1780–1790, 2014.

[5] R. Vazquez, F. Galivan, and E. F. Camacho, "Pulse-width predictive control for LTV systems with application for spacecraft rendez-vous," *Control Eng. Pract.*, vol. 60, pp. 199–210, 2017.

[6] C. Gazzino, C. Louembet, D. Arzelier, N. Jozefowiez, D. Losa, C. Pittet, and L. Cerri, "Integer programming for optimal control of geostationary station keeping of low-thrust satellites," LAAS Report 16341, July 2017.

[7] D. Zlotnik, S. Di Cairano, and A. Weiss, "MPC for coupled station keeping, attitude control, and momentum management for GEO satellites using on-off electric propulsion," in *P. IEEE Conf. Contr. Techol. Appl.*, 2017, pp. 1835–1840.

[8] A. Weiss, U. V. Kalabić, and S. Di Cairano, "Station keeping and momentum management of low-thrust satellites using MPC," *Aerosp. Sci. Technol.*, no. 6, pp. 229–241, May 2018.

[9] R. J. Caverly, S. Di Cairano, and A. Weiss, "Split-horizon MPC for coupled station keeping, attitude control, and momentum management of GEO satellites using on-off electric propulsion," in *P. Amer. Contr. Conf.*, 2018, to appear.

[10] C. Gazzino, D. Arzelier, L. Cerri, D. Losa, C. Louembet, and C. Pittet, "Solving the minimum-fuel low-thrust geostationary station keeping problem via the switching systems theory," in *European Conf. Aeronaut. Space Sci.*, July 2017.

[11] D. M. Goebel, J. E. Polk, I. Sandler, I. G. Mikellides, and J. R. Brophy, "Evaluation of 25-cm XIPS thruster life for deep space mission applications," in *P. Int. Elec. Propul. Conf.*, 2009.

[12] E. M. Soop, *Handbook of Geostationary Orbits*. Springer, 1994.

[13] H. Marquez, *Nonlinear Control Systems*. Hoboken, NJ: John Wiley & Sons, 2003.

[14] A. Weiss, I. Kolmanovsky, D. S. Bernstein, and A. Sanyal, "Inertia-free spacecraft attitude control using reaction wheels," *J. Guid. Control Dynam.*, vol. 36, no. 5, pp. 1425–1439, 2013.

[15] A. H. J. de Ruiter, C. J. Damaren, and J. R. Forbes, *Spacecraft Dynamics and Control: An Introduction*. Chichester, West Sussex, UK: John Wiley & Sons, 2013.